



Air permeability of biochar-amended clay cover

Ming-Yu Li¹ · Wen-Jing Sun¹ · Ye-Jiao Wang¹ · De-An Sun¹ · Yun-Zhi Tan²

Received: 25 September 2020 / Accepted: 22 March 2021 / Published online: 16 April 2021
© Saudi Society for Geosciences 2021

Abstract

Biochar has a porous structure with high specific surface area and high adsorption. Moreover, it provides a suitable habitat for microorganisms that can reduce harmful gases. Adding biochar to a traditional landfill clay cover (i.e., biochar-amended clay cover) can increase soil porosity, improve soil air flow, and reduce landfill methane emissions which are an area of interest for many researchers. In the present research, the air permeability of biochar-clay is considered to be the main measure in evaluating the fluid-flow characteristic of the material. We discussed the influence of biochar content and particle size on air permeability of biochar-clay and its mechanism. The air permeability coefficient k_a of biochar-clay mixture with different biochar content (0%, 5%, 10%, 15%, and 20%), dry densities (1.42 g/cm³, 1.56 g/cm³, and 1.65 g/cm³), and biochar particle size ranges (<74 μm, 20~40 μm, 40~74 μm, and >74 μm) were measured using a flexible wall air permeability testing device. Changes in soil pore structure were analyzed by scanning electron microscopy (SEM) and nuclear magnetic resonance (NMR). The results show that when dry density was 1.42 g/cm³, the air permeability coefficient decreased as the biochar content increased. For biochar-clay mixture of 1.56 g/cm³ and 1.65 g/cm³, when the biochar content was 15%, the air permeability coefficient of biochar-clay mixture reached its lowest value. Comparing the air permeability coefficient of biochar-clay mixture with non-intersecting particle size groups of biochar, it was revealed that the permeability coefficient decreased as the biochar particle size decreased. Based on the pore structure of biochar-clay mixture with different biochar content and particle size, the influence biochar content and particle size on the air permeability was evident.

Keywords Biochar · Content · Particle size · Air permeability · Pore structure · Pore size distribution

Responsible Editor: Amjad Kallel

✉ Wen-Jing Sun
wjsun@shu.edu.cn

Ming-Yu Li
lmy20180718@shu.edu.cn

Ye-Jiao Wang
yejiaowang@shu.edu.cn

De-An Sun
sundean@shu.edu.cn

Yun-Zhi Tan
yztan@ctgu.edu.cn

¹ Department of Civil Engineering, School of Mechanics and Engineering Science, Shanghai University, Shanghai 200444, People's Republic of China

² College of Civil Engineering & Architecture, China Three Gorges University, Yichang 443002, China

Introduction

In many countries, sanitary landfill is the primary method used for municipal solid waste disposal (Chen and Ke 2005; Reddy et al. 2015). However, landfill gases are released with the decay of organic material during the landfill's service period. Generally, landfill gas contains two greenhouse gases—methane (55~60%) and carbon dioxide (40~45%)—and the global greenhouse effect potential of methane is approximately 25 times that of carbon dioxide (IPCC 2007). For small-to-medium-sized old landfills with no gas-collection system, some methane often escapes into the atmosphere. Even for larger landfills with an efficient gas collection system, 5~40% of methane can escape (US-EPA 2011). Hence, it is important to search for an economical, sustainable, and efficient material as the final cover layer of landfills in order to contain and reduce methane emissions.

In traditional landfills, compacted clay is widely used as the barrier layer (US-EPA 1989) because of its economic and simple construction process. However, owing to climate/environment changes, such as rainfall, sunshine, or uneven

settlement, shrinkage cracks may occur in the landfill's final cover soil, leading to the damage of its integrity and sealing (Omari et al. 1996; Sun and Cui 2020; Sun et al. 2020). It weakens the soil barrier. In recent years, biochar, a sustainable and environmentally friendly soil-amended material for a landfill's final cover, has drawn the considerable interests of researchers (Wong et al. 2016; Wong et al. 2017). With a well-developed pore structure, high chemical stability, and high cation exchange capacity (Lehmann 2007; Jeffery et al. 2011; Sun et al. 2020), biochar provides a suitable space for methane-oxidizing bacteria, promotes methane microbial oxidation-reduction (Yu et al. 2013; Sadasivam and Reddy 2015), and reduces landfill methane emissions.

Over the past few years, researchers have investigated on the air permeability of soils mixed with biochar. Oguntunde et al. (2010) and Sun and Lu (2014) showed that the addition of biochar increases the porosity of soils and consequently enhances the permeability of gases. Obia et al. (2016) found that total porosity increased by 2% when biochar was added. Amoakwah et al. (2017) conducted an air permeability test on sandy and mixed soils with 10 t ha⁻¹ and 20 t ha⁻¹ of biochar and found that relative gas diffusivity increased with increasing air-filled porosity. At low air-filled porosities, there was a tendency for larger permeability values for mixed soils with 20 t ha⁻¹ compared to sandy and mixed soils with 10 t ha⁻¹. Sun et al. (2013) showed that the addition of biochar changes the soil pore structure parameters—e.g., pore organization and pore connectivity-tortuosity—and causes a significant decrease in soil bulk density and an accompanying increase in total porosity. The soils in the above studies are chiefly agricultural soil, sandy soil, and sand, usually with a low dry density, in a loose state with a degree of compaction of about 65% (Mchenry 2011; Garg and Ng 2015). Garg et al. (2020) studied the air permeability of biochar-amended soils with different degrees of compaction and concluded that the air permeability of biochar-amended soil is relatively lower than that of soils without amendment, although a higher degree of compaction requires larger suction (or drying) to enhance air permeability. Garg et al. (2019) studied the change of the air permeability of unsaturated biochar-amended clay-sand mixed soil under different biochar contents (0%, 5%, and 10%). It is concluded that the air permeability coefficient k_a increased linearly with soil suction in a semi-log scale, regardless of the biochar content. The addition of 5% and 10% biochar decreases air permeability by up to 50% and 65%, respectively, compared to bare soil. Obour et al. (2019) investigated the impact of biochar application on soil water retention, air movement through soil, and the pore characteristics of soil without biochar and soil altered with 15 and 30 Mg ha⁻¹ of biochar. The results showed that the altered with 30 Mg ha⁻¹ significantly increased k_a at matric potentials -30 hPa relative to amended with 15 Mg ha⁻¹. Cai et al. (2020) investigated the effect of soil suction and moisture content on gas

permeability for different biochar application percentages at high degree of compaction. The results show that with 5% and 10% of biochar, the decrease in gas permeability is around 50% and 65% compare with soil without biochar. Wong et al. (2016) found that biochar-amended soils can be used as an alternative landfill final cover. When the biochar is mixed into clay as an altered material for the landfill's cover layer, a higher degree of compaction is required to prevent the landfill gas from migrating to the atmosphere. At present, few studies on the air permeability characteristics of biochar-amended clay have been conducted. Wong et al. (2016) suggested that the effect of the particle size distribution of biochar on the air permeability of biochar improved soil should be investigated because the particle size of biochar significantly affects its physicochemical properties. Chen et al. (2020) studied the change of the air permeability of unsaturated biochar-amended silty sand mixed soil under four different sizes (<0.25, 0.25–1, 1–2, and >2 mm). It is found that the particle size of biochar played a significant role in altering soil microstructures. The addition of smaller biochar particles (i.e., <0.25 mm) decreased soil mesopores and macropores by 19%, resulting in a decrease in k_a of biochar-amended soil by 31% compared with the control. However, the addition of biochar with particle size >0.25 mm led to an increase in k_a of biochar-amended soil by up to 28–93% relative to the control. Sun et al. (2013) revealed that the impact of the incorporation of biochar on the number and structure of soil pores, which is the key factor affecting the air permeability of the soil, and the long-term effect between biochar and soil, may influence air permeability. Thus, from the above studies, we can see that biochar content and particle size can affect particle distribution and moisture distribution in soil and then affect the pore structure and porosity of soil, which are related to the permeability of soil (Kallel et al. 2004; Kallel et al. 2006). However, a detailed understanding of the mechanisms underlying the changes in the physical structure of the soil after the application of biochar are still lacking (Lehmann et al. 2009; Atkinson et al. 2010).

In this paper, the air permeability coefficient k_a was measured using a flexible wall air permeability testing device on biochar-clay mixture with different dry densities (1.42 g/cm³, 1.56 g/cm³, and 1.65 g/cm³), biochar content (0%, 5%, 10%, 15%, and 20%), and biochar particle size (>74 μm, 40–74 μm, 20–40 μm, and <74 μm), and the variations of the air permeability can be obtained. The pore structure of the biochar-clay mixture samples were measured using a scanning electron microscope (SEM) and nuclear magnetic resonance (NMR), and the effect of biochar content and particle size on air permeability was thus analyzed at the micro-level. The present study provides a reference for determining suitable biochar proportions and design parameters for a cover layer amended with biochar in landfills.

Materials and methods

Test materials and specimen preparation

The biochar used in this study was produced by pyrolysis of rice straw under oxygen-limited conditions at 500 °C. The skeleton structure of the original biomass was not damaged during the high-temperature pyrolysis process, and the microstructure of the biochar was well preserved. The basic physicochemical properties of clay and biochar used in the test are listed in Table 1. Figure 1 shows the morphological characteristics of the tested biochar after using a SEM. Biochar's porous structure can be seen from the micro-morphology of the rice straw biochar. According to the standard test method for chemical analysis of wood charcoal (ASTM D 1762-84 2007), the ash content of the biochar was 18.80%. To obtain the mass loss rate, 20g of biochar was placed in a muffle furnace at a temperature of 800 °C for 4h, and the quality loss was obtained.

To study the effect of biochar particle size on the air permeability of biochar-clay mixture, the original biochar was ground in a ball mill for 40 min and sieved with different pore diameters (200 mesh, 400 mesh, and 800 mesh). The sizes of 200 mesh, 400 mesh, and 800 mesh are 74 μm, 40 μm, and 20 μm, respectively, as shown in Fig. 2. Four biochar specimens with particle sizes of >74 μm, 40~74 μm, 20~40 μm, and <74 μm were obtained. Figure 3 shows the grain size distribution of clay and the aggregate size distributions of the above four biochar specimens with different particle sizes.

Five biochar-clay soil specimens were prepared with a biochar mass percentage of 0%, 5%, 10%, 15%, and 20%, respectively. The dry densities were 1.42 g/cm³, 1.56 g/cm³, and

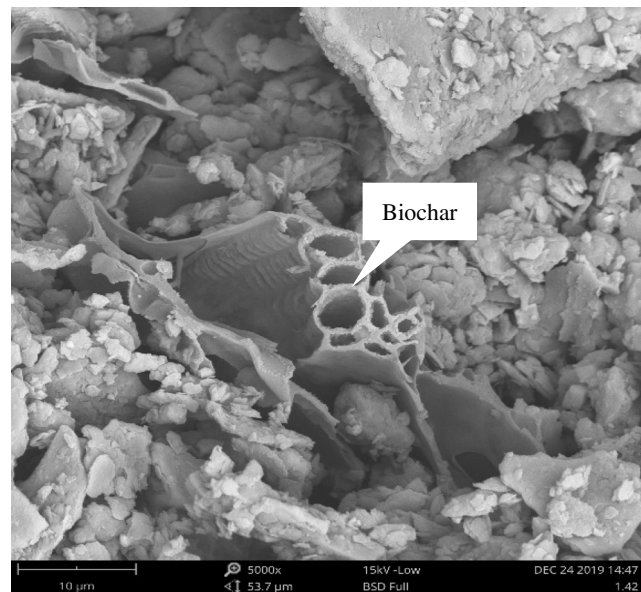


Fig. 1 Morphological characteristics of biochar in the experiment

1.65 g/cm³, respectively, or 85%, 95%, and 100% of the clay's maximum dry density, respectively. According to the Technical code for municipal solid waste sanitary landfill closure (GB 51220 2017), the degree of compaction of the landfill cover soil is not less than 90% of the standard proctor maximum dry density (SPMDD) of clay, according to the standard (GB 51220 2017), and the compactness of the slope is not less than 85%. The weighed biochar and dry soil were thoroughly mixed. Then the mixed soil specimens were mixed with deionized water and sealed in polyethylene bags for 24h. Finally, the mixed soil specimens were placed in a sampler and compacted with a jack to prepare compacted samples with a diameter of 6.18 cm, a height of 4.00 cm at an initial water content of 14.0%. Table 2 shows the initial state of the air permeation test sample. Table 3 shows the particle relative density of biochar-clay mixture with different particle sizes.

Considering the influence of biochar content on the air permeability coefficient of biochar-clay mixture, the particle size of biochar used was <74 μm, and the dry density was 1.65 g/cm³, 1.56 g/cm³, and 1.42 g/cm³. Under the influence of biochar particle size, the biochar content and dry density of samples were 10% and 1.56 g/cm³, and the biochar particle size >74 μm, 40~74 μm, 20~40 μm, and < 74 μm, respectively.

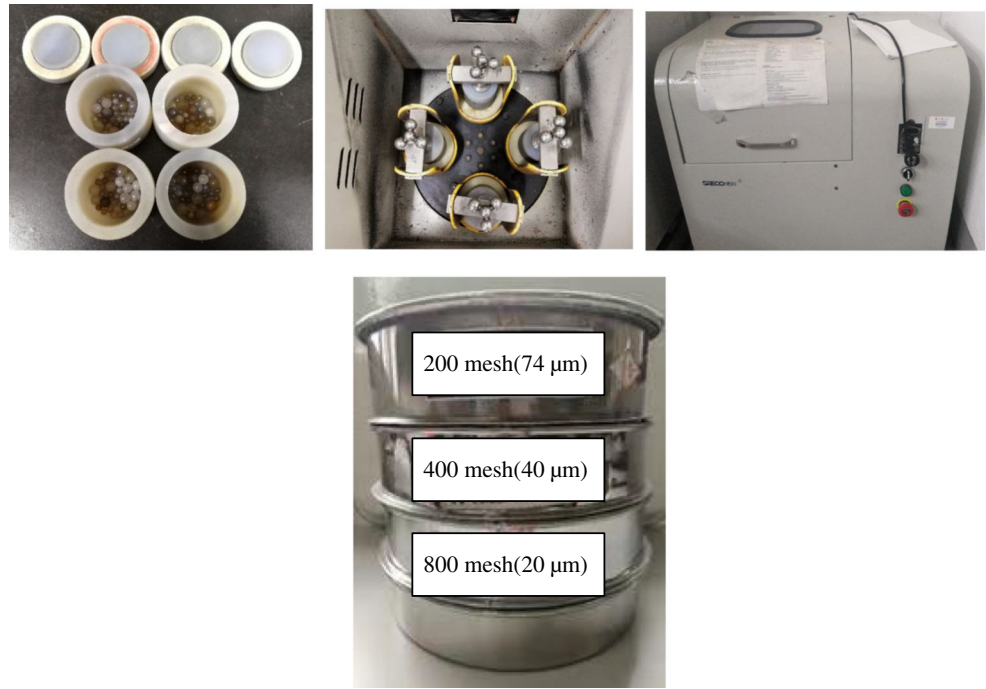
Measurement of air permeability

Figure 4 shows the test device to measure the air permeability coefficient. The device consists primarily of five parts: compressed air supply, digital display voltage regulator, water pressure controller, air tank, pressure chamber, and U-shaped manometer. The air inlet at the bottom of the pressure chamber was connected to the air tank, and the air tank's other

Table 1 Basic physical and chemical indexes of clay and biochar

Clay	
Atterberg limits	
Liquid limit (LL/%)	35.98
Plastic limit (PL/%)	22.20
Plastic index (PI)	13.78
Max. dry density (g/cm ³)	1.65
Optimum water content w_{opt} (%)	22.50
Specific gravity	2.67
pH	7.70
CEC (cmol kg ⁻¹)	10.70
Biochar	
Specific gravity	1.99
Specific surface area (SSA m ² /g)	385.60
pH	10.00
Ash content (%)	18.80

Fig. 2 Preparation of biochar with four biochar particle sizes



end was connected to a compressed air supply. A digital display voltage regulator was set between the air tank and the compressed air supply to regulate the pressure. It should be noted that a small amount of water was placed in the air tank to approach the sample humidity. The test method is similar to that used by Yoshimi and Osterberg (1963) and Delage et al. (1998). It has been shown that when the air pressure is less than 8 kPa, the results of air permeability measured by using Fick’s law and Darcy’s law are similar, and the effects of air compressibility can be ignored (Yoshimi and Osterberg 1963; Blight 1971). At the beginning of the test, a confining pressure of 40 kPa was applied in the pressure chamber before the test. The air permeability test began after the air pressure of the U-shaped manometer stabilized at the set pressure value (approximately 7.8 kPa) for 2 min. At the beginning of the test ($t = 0$),

we opened the valve that connects the bottom of the pressure chamber. This induced an air flow through the specimen. We then recorded the height of the liquid level of the U-shaped manometer at different times (Wang et al. 2017; He et al. 2017). It should be noted that the water content, mass, and volume are re-measured after test.

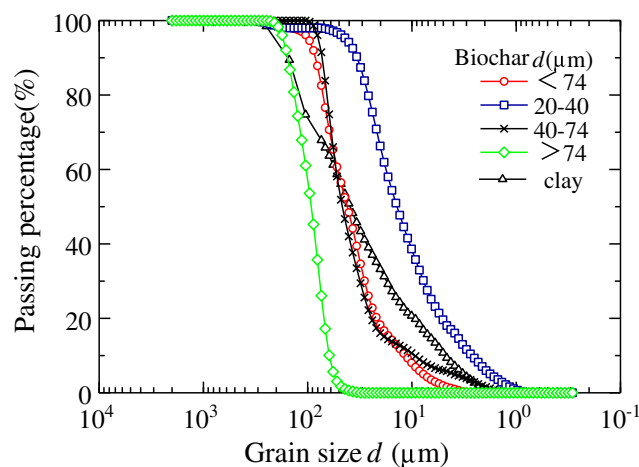


Fig. 3 Grain size distribution of clay and four biochar particle sizes

Table 2 Air permeability test sample initial state

α (%)	d (μm)	w (%)	ρ_d (g/cm^3)	e	S_r (%)
0	<74	14	1.42	0.89	42.00
5	<74	14	1.42	0.86	42.83
10	<74	14	1.42	0.85	43.06
15	<74	14	1.42	0.82	44.13
20	<74	14	1.42	0.79	45.09
0	<74	14	1.56	0.71	52.39
5	<74	14	1.56	0.70	53.15
10	<74	14	1.56	0.67	54.68
15	<74	14	1.56	0.65	55.39
20	<74	14	1.56	0.64	55.92
0	<74	14	1.65	0.61	60.85
5	<74	14	1.65	0.60	61.95
10	<74	14	1.65	0.57	63.43
15	<74	14	1.65	0.55	64.92
20	<74	14	1.65	0.53	66.78
10	>74	14	1.56	0.67	54.20
10	40-74	14	1.56	0.68	53.65
10	20-40	14	1.56	0.68	53.85
10	<74	14	1.56	0.69	52.38

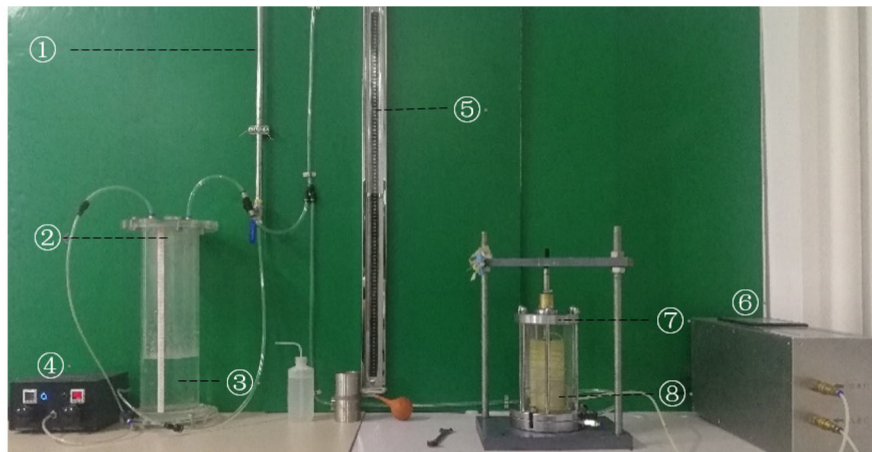
Table 3 Particle relative density of biochar-clay mixture with different particle sizes

Biochar content (α)	Biochar particle sizes d (mm)	ρ_s (g/cm ³)
5	>74	2.64
	40–74	2.64
	20–40	2.64
	<74	2.64
10	>74	2.61
	40–74	2.61
	20–40	2.61
	<74	2.60
15	>74	2.58
	40–74	2.58
	20–40	2.58
	<74	2.57

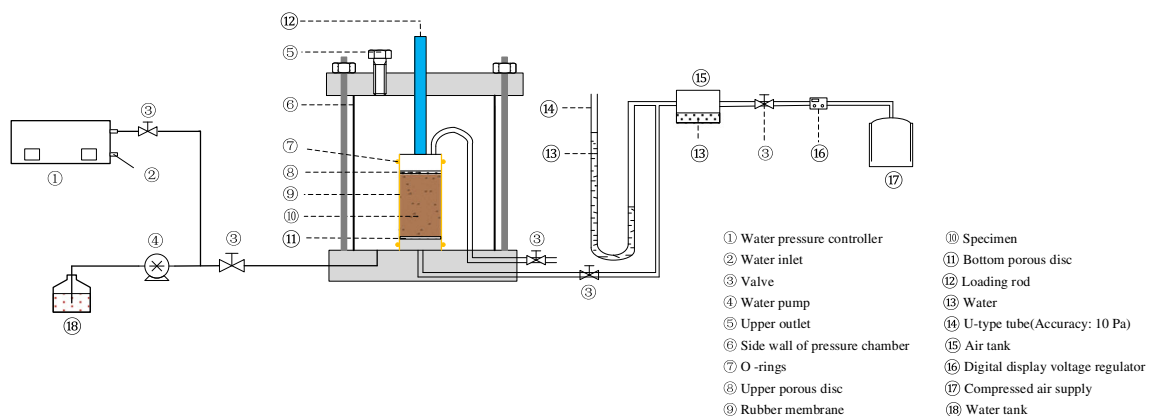
Based on Darcy’s law, Yoshimi and Osterberg (1963) deduced and proved that $\log[P(t)/P(0)]$ —e.g., the logarithm of the ratio of pressure $P(t)$ to initial pressure $P(0)$ —at t time presents a linear relationship with time t . It also gives the formula for calculating the air permeability coefficient k_a based on the linear slope.

$$k_a = -\frac{2.3Vh\mu_a}{t} \cdot \frac{\log \frac{P(t)}{P(0)}}{A \left[P_a + \frac{P(0)}{4} \right]} \tag{1}$$

where k_a is the air permeability coefficient (m²); h is the specimen thickness (m); A is the cross-sectional area of the specimen (m²); V denotes the air tank volume (m³); μ_a is the dynamic coefficient of viscosity of air at 20 °C temperature (1.796×10^{-5} Pa·s); and P_a is the atmospheric pressure (Pa).



①Compressed air supply ②Air tank ③Water ④Digital display voltage regulator ⑤U-shaped manometer(Accuracy: 10 Pa; Inner diameter:7 mm) ⑥Water pressure controller ⑦Pressure chamber ⑧ Specimen
(a)



(b)

Fig. 4 Experimental set-up for air permeability test. **a** Picture of the air permeation test device. **b** Sketch of the air permeability measurement system

Microstructure analyses

The microstructure and pore size distribution of biochar-clay mixture with different biochar content and particle size were measured using a Quanta FEG450 field emission scanning electron microscope (SEM) and a Macro MR12-110H-1, which is a nuclear magnetic resonance (NMR) scanning device. The variation of the air permeability coefficient of biochar-clay mixture of varying biochar content and particle size was analyzed at a micro-level. The specimens were frozen by immersion in liquid nitrogen ($-195\text{ }^{\circ}\text{C}$) for 5 min before SEM scanning (Gallé 2001) and then placed in a Labconco freeze dryer for vacuum cold drying. The freeze-dried specimens were pasted onto a copper sheet using conductive tape and the surface sprayed with gold. The sheet was then placed on the sample table of the SEM test instrument for scanning and photographing.

The magnetic field strength of the permanent magnet unit is 0.3T (Tesla). The temperature of the magnet unit is maintained at $32\text{ }^{\circ}\text{C}$, with a variation of $\pm 0.01\text{ }^{\circ}\text{C}$ to ensure the uniformity and stability of the main magnetic field in the test. Moreover, the effective test area of the sample tube is 60 by 60 mm ($h \times d$, where h and d are the height and diameter of the sample tube, respectively). The echo time is 0.2 ms; the repetition time is 1000 ms, and the number of echoes is 2000.

A T_2 distribution curve can be obtained by the NMR test. T_2 describes the decay speed of the transverse magnetization, which is the transverse relaxation time. Olumide et al. (2009) and Tian et al. (2018) point out that the value of T_2 is directly proportional to the pore radius r . Hence, the value of T_2 can be used to reflect the pore structure of the soil specimens. Assuming that the shape of the pores in the soil sample is spherical, the relationship between T_2 and r can be expressed as,

$$\frac{1}{T_2} \approx \rho_2 \left(\frac{3}{r} \right)_{\text{pore}} \quad (2)$$

where ρ_2 is the lateral transverse relaxation rate that is bound up with the soil's physical and chemical properties (Coates et al. 1999). The specimen was vacuum saturated before the NMR test. Therefore, the T_2 spectrum distribution curve of the saturated specimen can reflect the pore content in the specimen.

Results

Air permeability of biochar-clay mixture with different biochar content

Figure 5 shows that there is a linear relationship between $-\log(p_t/p_0)$ and t with different biochar content. Obviously,

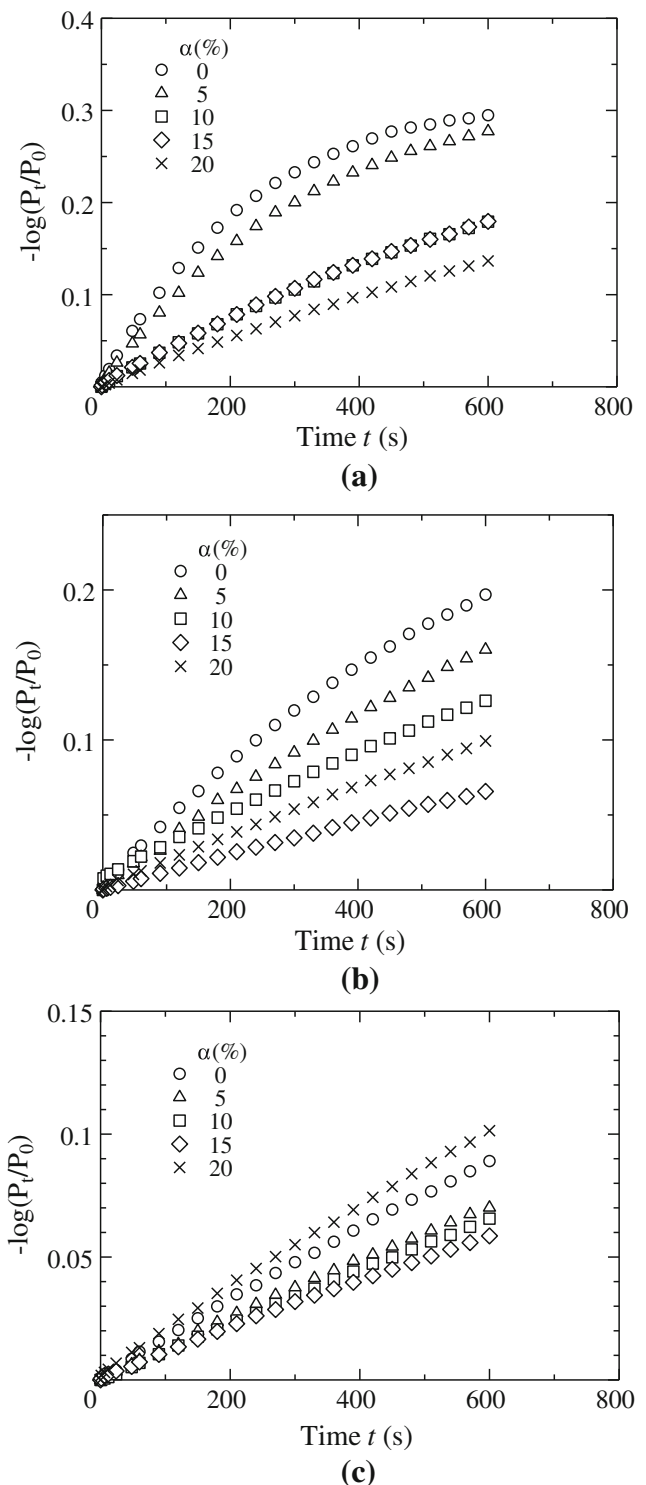


Fig. 5 Relationship between $-\log(p_t/p_0)$ and time t with different biochar content. **a** $\rho_d = 1.42\text{ g/cm}^3$; **b** $\rho_d = 1.56\text{ g/cm}^3$; **c** $\rho_d = 1.65\text{ g/cm}^3$

when the dry density is 1.42 g/cm^3 , the slope of the curve decreases with the increase of biochar content; when the dry density is 1.56 g/cm^3 and 1.65 g/cm^3 , with the increase of biochar content, the slope of the curve first decreases and then increases. Using the slope obtained in Fig. 5, the air

permeability coefficient of biochar-clay mixture with different biochar content is calculated by Eq. (1), as shown in Fig. 6.

Figure 6 shows the relationship between the air permeability coefficient k_a and the biochar content of biochar-clay mixture with dry densities of 1.65 g/cm³, 1.56 g/cm³, and 1.42 g/cm³ and particle sizes of <74 μm. It can be seen that the air permeability coefficient of the soils decreases continuously as the biochar content increases when the dry density is 1.42 g/cm³. However, when the dry densities are 1.56 g/cm³ and 1.65 g/cm³, not less than 90% of the Standard Proctor Maximum Dry Density (SPMDD) of clay, according to the standard (GB 51220 2017), the air permeability coefficient first decreases and then increases; that is, there is an amount of biochar that minimizes the permeability coefficient of the mixed soils. It can be speculated that there may be an optimal amount of biochar, which would be verified by testing the permeability coefficient of mixed soil samples with more biochar content. When the biochar content is less than 15%, the air permeability coefficient decreases as the biochar content increases, and the trend is more obvious at the lower dry density. For example, the air permeability coefficient of the specimen with a dry density of 1.56 g/cm³ decreases faster. For the specimen with a dry density of 1.56 g/cm³, the air permeability coefficient k_a of biochar content $\alpha = 0\%$ is $1.26 \times 10^{-14} \text{ m}^2$, while the air permeability coefficient k_a of $\alpha = 15\%$ is $4.23 \times 10^{-15} \text{ m}^2$, which decreases by one order of magnitude. However, when the dry density is 1.65 g/cm³ and the biochar content is less than 15%, the decreasing rate in the air permeability coefficient of the mixed soils is relatively low as the biochar content increases. When the biochar content is larger than 15%, the air permeability coefficient increases as the biochar content increases, and the effect of dry density on the air permeability coefficient decreases. For example, when the biochar content is 20%, the air permeability coefficient k_a of the specimens with different dry densities is similar.

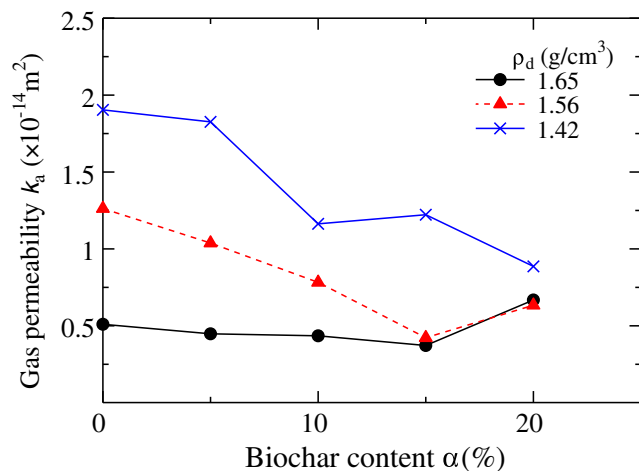
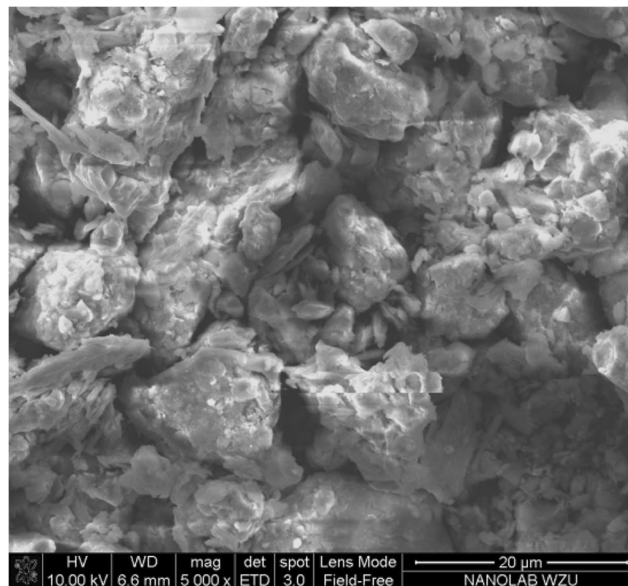
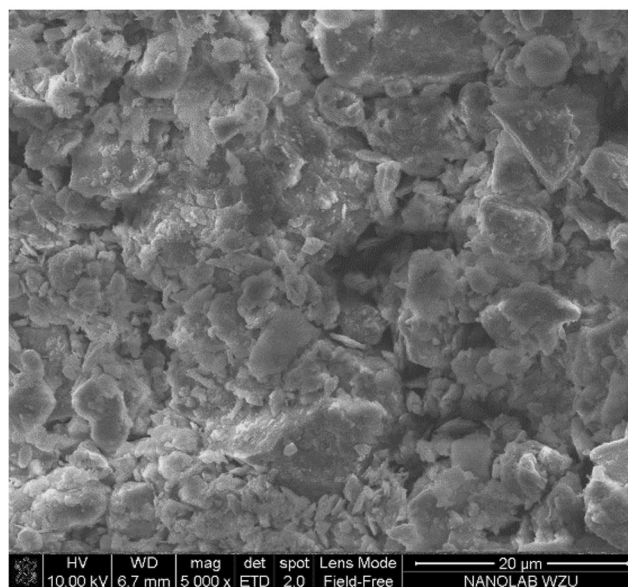


Fig. 6 Air permeability coefficient of biochar-clay mixture with different biochar content ($d < 74 \mu\text{m}$)

Figure 7 shows the SEM microstructure of pure clay and biochar-clay mixture with 15% biochar content. From the microscopic pore structure of pure clay in Fig. 7a, it can be seen that the clay particles form clay aggregates through cementation, which contact each other and rearrange to form a new pore structure. The pores of pure clay include inter- and intra-aggregate pores. Figure 7 b shows the microscopic pore structure of biochar-clay mixture with 15% biochar content under the same magnification. The figure shows that the particles of the mixed soil are evenly distributed and dense. The number of clay aggregates is reduced as are the specimens' pores. This shows that biochar can fill the pores between the clay aggregates.



(a)



(b)

Fig. 7 SEM images of biochar-clay mixture with different biochar content ($d < 74 \mu\text{m}$). a $\alpha = 0\%$, b $\alpha = 15\%$

Figure 8 a shows the T_2 spectrum distribution curve of biochar-clay mixture (0%, 5%, 10%, 15%, and 20% biochar content) with a biochar particle size $< 74 \mu\text{m}$ and dry density of 1.56g/cm^3 . When the biochar content is 0%, 5%, 10%, 15%, and 20%, the corresponding signal intensity are 117.04, 100.89, 93.66, 32.65, and 49.73, respectively. It can be obtained that the signal intensity first decreases and then increases. When $\alpha < 15\%$, the signal intensity decreases as the biochar content increases. However, when $\alpha > 15\%$, the signal intensity increases. The area of the T_2 distribution curve and horizontal axis reflects the content of hydrogen protons in soil pores (Tian et al. 2018). For saturated specimens, the area of the T_2 spectrum is proportional to the amount of fluid in the specimen pores. This means that the area of the T_2 distribution curve and horizontal axis can reflect the number of pores in the specimens. Figure 8 b shows the relationship between the area of the T_2 distribution curve of biochar-clay mixture and the biochar content. It can be seen that the area begins to decrease with the

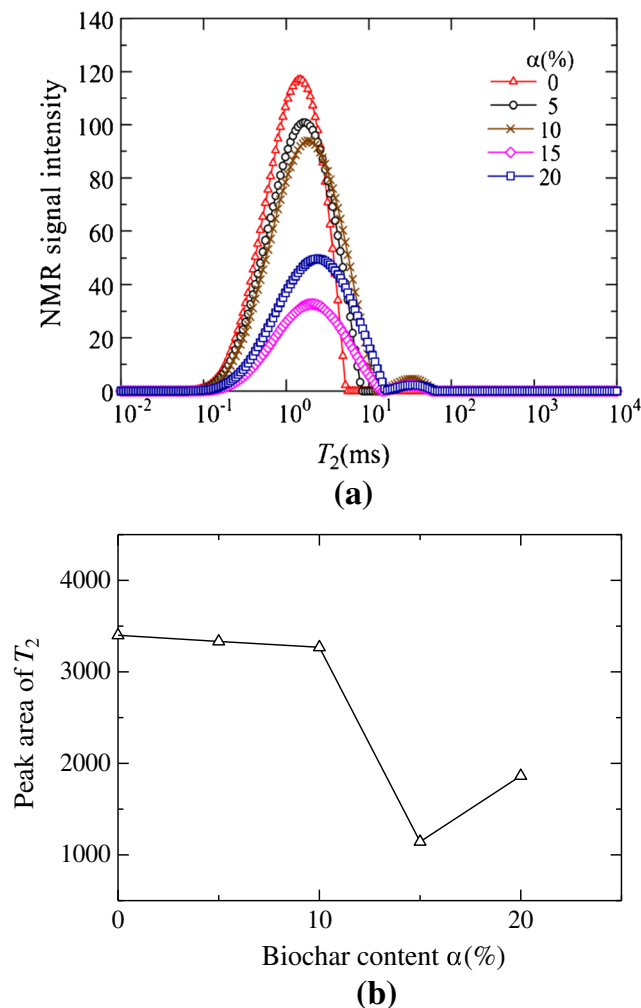


Fig. 8 T_2 test results of biochar-clay mixture with different biochar content. **a** T_2 distribution curves of biochar-clay mixture with different biochar content ($\rho_d = 1.56 \text{g/cm}^3$). **b** The peak area T_2 distribution curves of biochar-clay mixture with different biochar content ($d < 74 \mu\text{m}$)

increase of biochar content and decreases to its lowest when the biochar content is 15%. The area of the T_2 distribution curve becomes larger for $\alpha = 20\%$. In other words, the pore content in the soils first decreases and then increases.

Air permeability of biochar-clay mixture with different biochar particle sizes

Figure 9 shows that there is a linear relationship between $\log(p_i/p_0)$ and t with different particle sizes. It can be seen from the figure that the slope of $\log(p_i/p_0)$ and t curve of biochar-clay mixture increases with the increase of biochar non-intersecting particle size groups.

Figure 10 shows the air permeability coefficient of biochar-clay mixture (1.56g/cm^3 dry density and 10% biochar content) with particle sizes of $>74 \mu\text{m}$, $40\sim 74 \mu\text{m}$, $20\sim 40 \mu\text{m}$, and $< 74 \mu\text{m}$, respectively. From Fig. 10, we see that the air permeability coefficient decreases linearly with the decreasing biochar particle size in the three non-intersecting particle size groups of $> 74 \mu\text{m}$, $40\sim 74 \mu\text{m}$, and $20\sim 40 \mu\text{m}$. When the particle size is $< 74 \mu\text{m}$, the permeability coefficient of biochar-clay mixture is smaller than the other three non-intersecting particle size groups. For example, when the dry density is 1.56g/cm^3 , the permeability coefficient of pure clay is $1.26 \times 10^{-14} \text{m}^2$, which is smaller than that of specimens mixed with $>74 \mu\text{m}$ particles of biochar ($k_a = 1.78 \times 10^{-14} \text{m}^2$).

Figure 11 shows the NMR test results of biochar-clay mixture with dry density of 1.56g/cm^3 , 15% biochar content, and particle size of $>74 \mu\text{m}$, $40\sim 74 \mu\text{m}$, $20\sim 40 \mu\text{m}$, and $<74 \mu\text{m}$, respectively. Firstly, the T_2 spectral distribution curves of $20\sim 40 \mu\text{m}$, $40\sim 74 \mu\text{m}$, and $>74 \mu\text{m}$ are compared with non-intersecting particle size groups of biochar. The T_2 distribution curves of $20\sim 40 \mu\text{m}$ and $40\sim 74 \mu\text{m}$ are a unimodal structure, and the T_2 value corresponding to the peak of T_2 spectrum is 1.20 ms and 1.38 ms, respectively. The T_2 distribution curve with particle size $>74 \mu\text{m}$ has a bimodal structure. The first

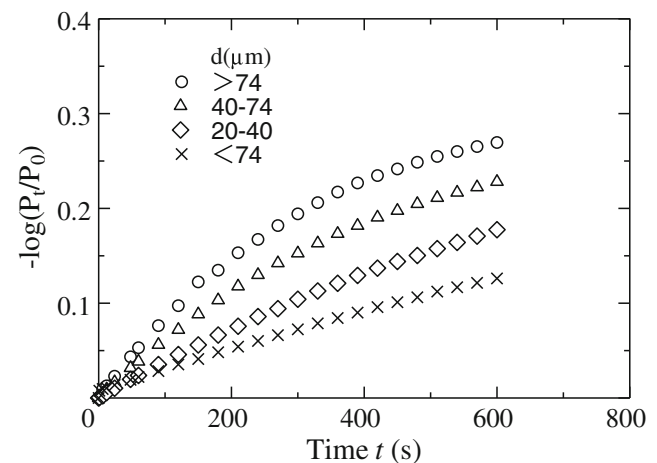


Fig. 9 Relationship between $-\log(p_i/p_0)$ and time t under different particle sizes ($\rho_d = 1.56 \text{g/cm}^3$, $\alpha = 10\%$)

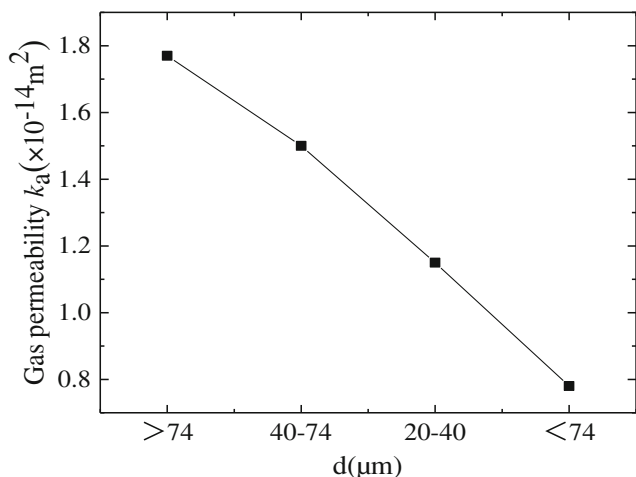


Fig. 10 Air permeability coefficient of biochar-clay mixture with different biochar particle sizes ($\alpha = 10\%$)

peak is close to the two previous peaks, and the T_2 value is 38.72 ms at the second peak with the span at 11.10~333.13 ms. The T_2 distribution reflects the pore-size distribution. Tian et al. (2018) showed that, when $T_2 < 60$ ms, the NMR test results reflect the water in small pores or micropores, and the corresponding pores are micropores; when T_2 is in the range of 60~300 ms, the corresponding pores are macropores.

For mixed biochar-clay mixture with particle sizes of 20~40 μm and 40~74 μm , their T_2 spectrum distribution curves are almost the same. The ranges of T_2 at main peak are 0.025~4.20 ms and 0.025~5.17 ms, respectively, and the corresponding pores are chiefly small pores and micropores. However, the T_2 value at peak of the 20~40 μm group moves to the left compared with that of the 40~74 μm group; that is, the most probable pore diameter—the pore diameter corresponding to the peak—is smaller than that of the 40~74 μm group. Moreover, the peak area decreases, that is, the number of small pores also decreases. Therefore, the air permeability coefficient of 20~40 μm biochar-clay mixture is less than that of 40~74 μm .

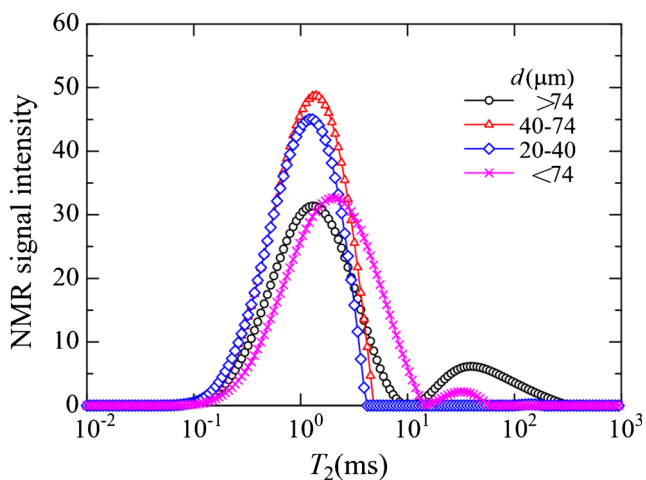


Fig. 11 T_2 distribution curves of biochar-clay mixture with different biochar particle sizes ($\rho_d = 1.56 \text{g/cm}^3$)

For the biochar-clay mixture with the particle size $>74 \mu\text{m}$, the soil has macropores, and the air permeability coefficient k_a of biochar-clay mixed soil is highest. For biochar with a mixed particle size of $<74 \mu\text{m}$, there exists some large carbon particles. Therefore, the spectral curve moves to the right and the pore diameter increases. But the amount of total porosity decreases obviously, which makes the air permeability coefficient a minimum.

According to the experiment and mechanism analysis of particle size and biochar content, the air permeability coefficient k_a of biochar-clay mixture is the lowest when the biochar content is 15% and the particle size $<74 \mu\text{m}$.

Discussion

Through the air permeability test results of biochar-clay mixture with different biochar content and biochar particle size, it can be observed that the air permeability is related to many factors, such as biochar content, degree of compaction, and the particle size distribution of soil, including the particle size of biochar and the relative particle size of biochar and clay.

Effect of biochar content on air permeability of biochar-clay mixture

Wong et al. (2016) observed the effects of the biochar content and degrees of compaction on air permeability and illustrated that the soil-biochar interactions had a significant impact on the air transport behavior in compacted biochar-clay.

The air permeability coefficient of the biochar-clay mixture decreases continuously as the biochar content increases when the dry density is 1.42g/cm^3 , as shown in Fig. 6. This is because the gaps between the clay aggregates are partly filled by the biochar. The smaller the dry density, the more the inter-aggregate pores in the clay. Some of these pores are filled with biochar particles, and the soil becomes dense. It can be obtained from Fig. 1 that the pores between clay aggregates are partly filled with biochar. The air permeability coefficient of the specimens gradually decreases as the biochar content increases. The higher the biochar content, the more significant the filling effect. Hence, the permeability coefficient of mixed soil decreases significantly as the biochar content increases.

However, for specimens with a dry density not less than 90% of the maximum dry density of clay, such as those of 1.56g/cm^3 and 1.65g/cm^3 , the air permeability coefficient first decreases and then increases. The reason may be that with increasing biochar content, part of the biochar occupies the clay particle pores and fills the pores in the internal structure of the soil, and the other part of the biochar is dispersed in clay agglomeration. The air permeability coefficient rises with an increase in biochar content since biochar is a loose and porous material. Moreover, at low biochar content (i.e., $\alpha < 15\%$), the

impact of compactness is greater, but it is smaller at higher biochar content (i.e., $\alpha > 15\%$). The reason is that there are more inter-pores of clay aggregates at low compaction. After adding biochar, the filling effect is more obvious, and the air permeability coefficient of the specimen decreases greatly. With the increase of biochar content ($\alpha > 15\%$), some biochar particles fill the pores between soil particles, and some carbon particles contact with each other to form a carbon skeleton. The porosity of biochar can improve the permeability coefficient of soil. At this time, the filling effect of biochar has less effect, and the porosity of biochar plays a leading role in the air permeability; therefore, the air permeability coefficient increases. The phenomenon can be explained by NMR results, as shown in Fig. 8b. At higher dry density of 1.56g/cm^3 , the area of the T_2 distribution curve first decreases and then increases. This reveals the mechanism of the variation of the air permeability coefficient with biochar content changing for mixtures with higher dry density at the level of the microscopic pore structure.

The results of this study were not consistent with those presented by previous researchers (Sun et al. 2013; Amoakwah et al. 2017; Garg et al. 2019). Sun et al. (2013) revealed that the air-filled porosity was markedly greater in the biochar-amended soil than in the reference soil. The air permeability is related to the air-filled porosity of soils. Under the same dry density, the relationship between air permeability coefficient and void ratio of biochar-clay mixture is shown in Fig. 12. The results show that the addition of biochar decreases the void ratio of the biochar-clay mixture. This decrease in void ratio is the result of the change in the overall solid density due to increase in biochar content. It is known that the permeability of soil is often related to the void ratio; therefore, decrease in air permeability as shown in Fig. 6 can be explained and related to the change in void ratio. When the dry density is 1.56g/cm^3 and 1.65g/cm^3 , with the increase of biochar content ($\alpha > 15\%$), some biochar particles fill the pores between soil particles, and some carbon particles contact

with each other to form a carbon skeleton. The porosity of biochar can improve the permeability coefficient of soil. At this time, the filling effect of biochar has less effect, and the porosity of biochar plays a leading role in the air permeability; therefore, the air permeability coefficient increases. Water content has a significant effect on air permeability. Porosity can also influence air permeability. The relationship between degree of saturation and air permeability coefficient can reflect the influence of water content and porosity synthetically on the air permeability coefficient of mixed soil, as shown in Fig. 13. It can be seen from the figure that with the decrease of saturation, the air permeability coefficient has a gradually increasing trend. The air permeability of biochar-amended soil was higher than that in non-amended soil. Previous studies mainly focused on the application of biochar to agricultural soil, such as sandy loam and silty clay. In addition, agricultural soil usually has a low degree of compaction to benefit root growth (Mchenry 2011; Garg and Ng 2015). However, it is aimed at the final cover of landfills in this research, which requires a high degree of compaction, not less than 90% of the standard proctor maximum dry density (SPMDD), according to the standard (GB 51220 2017). At this time, the degree of compaction, the biochar content, and the relative particle size of clay and biochar can affect the air permeability coefficient of specimens. But the influence of the relative particle size of biochar and clay on the air permeability is more significant. This is because of the influence of the relative particle size of biochar and clay on the micropore structure of soils. For clay whose particle size is smaller than or equal to that of biochar, biochar may exist as a part of the soil skeleton of the mixed soils, which increases the porosity of soil and subsequently air permeability. However, for materials whose particle size is larger than that of biochar, biochar is filled in the particle pores as filler. Hence, the porosity of soil decreases and subsequently the air permeability of the mixed soils decreases.

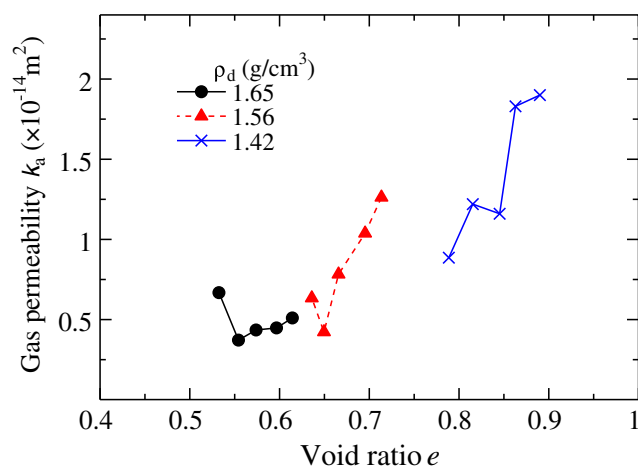


Fig. 12 Air permeability coefficient of biochar-clay mixture with different void ratios ($d < 74\ \mu\text{m}$)

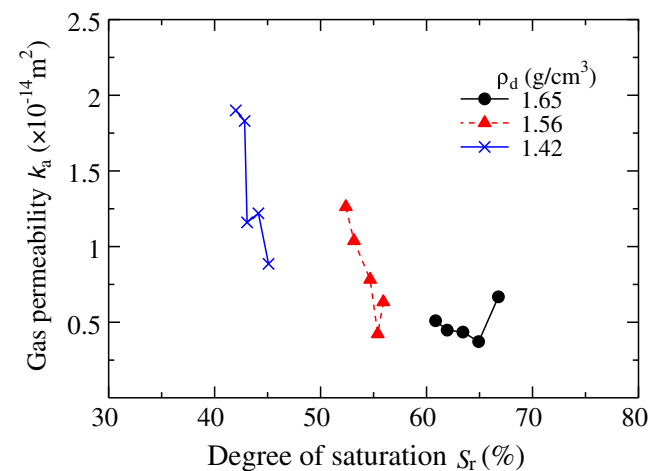


Fig. 13 Air permeability coefficient of biochar-clay mixture with different degrees of saturation ($d < 74\ \mu\text{m}$)

Effect of biochar particle size on air permeability of biochar-clay mixture

The air permeability coefficient decreases linearly with decreasing biochar particle size in the three non-intersecting particle size groups of $>74\ \mu\text{m}$, $40\text{--}74\ \mu\text{m}$, and $20\text{--}40\ \mu\text{m}$. When the particle size is $<74\ \mu\text{m}$, the permeability coefficient of biochar-clay mixture is smaller than the other three non-intersecting particle size groups. The results indicate that the addition of biochar with a large particle size can improve the soil's permeability. With the decrease of the particle size of biochar, the small size biochar fills the pores in the internal structure of the clay, and the filling effect is better. As a result, the soil becomes relatively dense, as shown in Fig. 6b, and the air permeability coefficient gradually decreases. For the biochar of particle size $<74\ \mu\text{m}$, it is a mixed particle size group, and the distribution of carbon particles is relatively uniform. However, there are carbon particles with particle size $< 20\ \mu\text{m}$, as shown in Fig. 3; therefore, the filling effect of biochar on clay pores improves under this particle size group. For the large particle size group with biochar particles $>74\ \mu\text{m}$, the pores in the soil increase after being mixed, and hence, the permeability coefficient is higher. The relative particle size of biochar and clay can also affect the air permeability coefficient of biochar-clay mixed soil. Chen et al. (2019) and Wong et al. (2018) studied the optimal pore size distribution of clay which is between 0.01 and $1\ \mu\text{m}$ from MIP results of clay, that is, the pore size of those pores with maximum probability. According to these results, the biochar particles $>74\ \mu\text{m}$ is larger than that of clay; therefore, it can be judged that the biochar acts as the soil skeleton in the mixtures. Therefore, the porosity of biochar-clay mixture increases, which leads to the increase of the air permeability.

To sum up, the air permeability coefficient of biochar amended soils is related to the micropore structure of soils, which is connected to the biochar content and particle size, the degree of compaction, and the relative particle size of biochar and clay.

Conclusion

The air permeability of biochar-clay mixture with different biochar content and particle sizes was measured using a flexible wall air permeability testing device. Pore structure and pore size distribution of biochar-clay mixture were obtained using SEM and NMR tests, and the effect of biochar content and particle size on the air permeability of biochar-clay mixture were analyzed. Main conclusions are as follows:

- (1) The influence of biochar content on the air permeability of biochar-clay mixture varies with the degree of compaction. When the dry density is $1.42\ \text{g}/\text{cm}^3$, the air permeability coefficient decreases with the increase of biochar content;

when the dry densities are $1.56\ \text{g}/\text{cm}^3$ and $1.65\ \text{g}/\text{cm}^3$, with the increase of biochar content, the air permeability coefficient first decreases and then increases.

- (2) By comparing the air permeability coefficient of biochar-clay mixture with non-intersecting particle size groups, it is found that the air permeability coefficient decreases as the biochar particle size decreases. The air permeability coefficient of biochar-clay mixture with biochar particle size $< 74\ \mu\text{m}$ is lowest compared with other particle size groups.

Acknowledgements The authors are grateful to the National Sciences Foundation of China (Grant No. 41977214, 41572284) for the financial supports.

Declarations

Conflict of interest The authors declare that they have no competing interests.

References

- Amoakwah E, Frimpong KA, Okae-Anti D, Arthur E (2017) Soil water retention, air flow and pore structure characteristics after corn cob biochar application to a tropical sandy loam. *Geoderma* 307:189–197
- Atkinson CJ, Fitzgerald JD, Hipps NA (2010) Potential mechanisms for achieving agricultural benefits from biochar application to temperate soils: a review. *Plant Soil* 337(1–2):1–18
- ASTM D1762-84 (2007) Standard test method for chemical analysis of wood charcoal. ASTM International, West Conshohocken PA
- Blight GE (1971) Flow of air through soils. *J Soil Mech Found Div* 97(SM4):607–624
- Chen YM, Ke H (2005) Engineering characteristics of municipal solid wastes and geotechnical problems of landfills. *Eng Mechan* S1:119–126
- Cai WL, Kumar H, Huang S, Bordoloi S, Garg A, Lin P, Gopal P (2020) ANN model development for air permeability in biochar amended unsaturated soil. *Geotech Geol Eng* 38(3):1295–1309
- Chen M, Dai J, Liu X, Kang Y, Qin MJ, Wang ZT (2019) Contributions of pore-throat size distribution to reservoir quality and fluid distribution from NMR and MIP in tight sandy conglomerate reservoirs. *Arab J Geosci* 12(1):1–12
- Chen Z, Chen C, Kamchoom V, Chen R (2020) Gas permeability and water retention of a repacked silty sand amended with different particle sizes of peanut shell biochar. *Soil Sci Soc Am J* 84:1630–1641
- Coates GR, Xiao LL, Prammer MG (1999) NMR Logging principles and application. Halliburton Energy Services Publication, Houston
- Delage P, Cui YJ, De Laure E (1998) Air flow through an unsaturated compacted silt. In: Proceedings of the 2nd International Conference on Unsaturated Soils UNSAT:563–568
- Garg A, Huang H, Kushvaha V, Madhushri P, Kamchoom V, Wani I, Koshy N, Zhu HH (2020) Mechanism of biochar soil pore–gas–water interaction: gas properties of biochar-amended sandy soil at different degrees of compaction using KNN modeling. *Acta Geophysica* 68(1):207–217
- Garg A, Bordoloi S, Ni JJ, Cai WL, Maddibiona PG, Mei GX, Poulsen TG, Lin P (2019) Influence of biochar addition on air permeability in unsaturated soil. *Géotech Lett* 9(1):1–20

- Garg A, Ng CWW (2015) Investigation of soil density effect on suction induced due to root water uptake by *Schefflera heptaphylla*. *J Plant Nutr Soil Sci* 178(4):586–591
- Gallé C (2001) Effect of drying on cement-based materials pore structure as identified by mercury intrusion porosimetry: a comparative study between oven-, vacuum-, and freeze-drying. *Cem Concr Res* 31(10):1467–1477
- GB 51220 (2017) Technical code for municipal solid waste sanitary landfill closure. China Building Industry Press, Beijing
- He Y, Cui YJ, Ye WM, Conil N (2017) Effects of wetting-drying cycles on the air permeability of compacted Téguline clay. *Eng Geol* 228:173–179
- IPCC (Intergovernmental Panel on Climate Change) (2007) Special report on renewable energy sources and climate change mitigation. Cambridge University Press, New York
- Jeffery S, Verheijen FGA, Veldt MVD, Bostos AC (2011) A quantitative review of the effects of biochar application to soils on crop productivity using meta-analysis. *Agric Ecosyst Environ* 144(1):175–187
- Kallel A, Tanaka N, Matsuto T (2004) Gas permeability and tortuosity for packed layers of processed municipal solid wastes and incinerator residue. *Waste Manag Res* 22(3):186–194
- Kallel A, Tanaka N, Tojo Y, Matsuto T, Hanada S (2006) Oxygen intrusion into waste in old landfills of low organic content. *Waste Manag Res* 24(3):242–249
- Lehmann J (2007) Bio-energy in the black. *Front Ecol Environ* 5(7):381–387
- Lehmann J, Czimczik C, Laird D, Sohi S (2009) Stability of biochar in the soil. Chapter 11. In: Lehmann J, Joseph S (eds) *Biochar for Environmental Management Science and Technology*. Earthscan, London, pp 183–205
- Mchenry MP (2011) Soil organic carbon, biochar, and applicable research results for increasing farm productivity under Australian agricultural conditions. *Commun Soil Sci Plant Anal* 42(10):1187–1199
- Omari GH, Thomas JC, Brown KW (1996) Effect of desiccation racking on the hydraulic conductivity of a compacted clay pollution liner. *Water Air Soil* 89(1):91–103
- Oguntunde PG, Abiodun BJ, Ajayi AE, Giesen NVD (2010) Effects of charcoal production on soil physical properties in Ghana. *J Plant Nutr Soil Sci* 171(4):591–596
- Obia A, Mulder J, Martinsen V, Cornelissed G, Borresen T (2016) In situ effects of biochar on aggregation, water retention and porosity in light-textured tropical soils. *Soil Tillage Res* 155:35–44
- Obour PB, Danso EO, Yakubu A, Abenney-Mickson S, Sabi EB, Darrah YK, Arthur E (2019) Water retention, air exchange and pore structure characteristics after three years of rice straw biochar application to an acriso soil. *Sci Soc Am J* 83(6):1664–1671
- Olumide T, Saif A, Stefan I, Blunt MJ (2009) Pore-scale simulation of NMR response. *J Pet Sci Eng* 67(3):168–178
- Reddy KR, Yargicoglu E, Yue D (2015) Enhanced microbial methane oxidation in landfill cover soil amended with biochar. *J Geotech Geoenviron* 140(9):194–198
- Sadasivam BY, Reddy KR (2015) Adsorption and transport of methane in landfill cover soil amended with waste-wood biochars. *J Environ Manag* 158:11–23
- Sun WJ, Cui YJ (2020) Determining the soil-water retention curve using mercury intrusion porosimetry test in consideration of soil volume change. *J Rock Mech Geotech Eng* 12(5):1070–1079
- Sun WJ, Li MY, Zhang WJ, Tan YZ (2020) Saturated permeability behavior of biochar-amended clay. *J Soils Sediments* 20(1):3875–3883
- Sun Z, Moldrup P, Elsgaard L, Arthur E, Bruun EW, Nielsed HH, Jonge LWD (2013) Direct and indirect short-term effects of biochar on physical characteristics of an arable sandy loam. *Soil Sci* 178(9):465–473
- Sun F, Lu S (2014) Biochars improve aggregate stability, water retention, and pore-space properties of clayey soil. *J Plant Nutr Soil Sci* 177(1):26–33
- Tian HH, Wei CF, Lai YM, Chen P (2018) Quantification of water content during freeze-thaw cycles: a nuclear magnetic resonance based method. *Vadose Zone J* 17(1):1–12
- US-EPA (United States Environmental Protection Agency) (2011) Available and emerging technologies for reducing greenhouse air emissions from municipal solid waste landfills. Office of Air and Radiation U.S. EPA. June
- US-EPA (United States Environmental Protection Agency) (1989) Technical guidance document: final covers on hazardous waste landfills and surface impoundments. US Environmental Protection Agency Washington
- Wang YJ, Cui YJ, Tang AM, Benahmed N, Duc M (2017) Effects of aggregate size on the compressibility and air permeability of lime-treated fine-grained soil. *Eng Geol* 228:167–172
- Wong JTF, Chen Z, Ng CWW, Wang MH (2016) Gas permeability of biochar-amended clay: potential alternative landfill final cover material. *Environ Sci Pollut Res* 23(8):7126–7131
- Wong JTF, Chen Z, Ng CWW, Wang MH (2017) Soil-water retention behavior of compacted biochar-amended clay: a novel landfill final cover material. *J Soils Sediments* 17(3):590–598
- Wong JTF, Chen Z, Wong AYY, Ng CWW, Wong MH (2018) Effects of biochar on hydraulic conductivity of compacted kaolin clay. *Environ Pollut* 234:468–472
- Yu L, Tang J, Zhang R, Wu QH, Gong MM (2013) Effects of biochar application on soil methane emission at different soil moisture levels. *Biol Fertil Soils* 49(2):119–128
- Yoshimi Y, Osterberg JO (1963) Compression of partially saturated cohesive soils. *J Soil Mechan Foundat Div* 89(4):1–24